HHS Public Access

Author manuscript

ACS Appl Mater Interfaces. Author manuscript; available in PMC 2019 May 16.

Published in final edited form as:

ACS Appl Mater Interfaces. 2018 May 16; 10(19): 16822–16835. doi:10.1021/acsami.8b04496.

Dual Suppression Effect of Magnetic Induction Heating and Microencapsulation on Ice Crystallization Enables Low-Cryoprotectant Vitrification of Stem Cell-Alginate hydrogel Constructs

Xiaoli Liu[a], **Gang Zhao**[a,*], **Zhongrong Chen**[a], **Fazil Panhwar**[a], and **Xiaoming He**[b,*]

[a]*Department of Electronic Science and Technology, University of Science and Technology of China, Hefei 230027, Anhui, China*

[b]*Fischell Department of Bioengineering, University of Maryland, College Park, MD 20742, USA*

Abstract

Stem cells microencapsulated in hydrogel as stem cell-hydrogel constructs have wide applications in the burgeoning cell-based medicine. Due to their short shelf life at ambient temperature, long-term storage or banking of the constructs is essential to their “off-the-shelf” ready availability needed for their widespread applications. As a high-efficiency, easy-to-operate, low-toxic and low-cost method for long-term storage of the constructs, low-cryoprotectant (CPA) vitrification has attracted tremendous attention recently. However, we found many cells in the stem cell-alginate constructs (~500 μm in diameter) could not attach to substrate post low-CPA vitrification with (~2 M penetrating CPAs). To address this problem, we introduced nano-warming via magnetic induction heating (MIH) of Fe_3O_4 nanoparticles to minimize recrystallization and devitrification during the warming step of the low-CPA vitrification procedure. Our results indicate that high-quality stem cell-alginate hydrogel constructs with an intact microstructure, high immediate cell survival (> 80%), and greatly improved attachment efficiency (nearly three times, 68% versus 24%) of the encapsulated cells could be obtained post-cryopreservation with nano-warming. Moreover, the cells encapsulated in the cell-hydrogel constructs post-cryopreservation maintained normal proliferation under 3D culture and retained intact biological functionality of multi-lineage differentiation. This novel low-CPA vitrification approach for cell cryopreservation enabled by the

[*]**Corresponding Author:** ZhaoG@ustc.edu.cn (G.Z.); shawnhe@umd.edu (X.H.).

Supporting information

The Supporting Information is available free of charge on the ACS Publications website at DOI:
Fabrication and collection of stem cell-hydrogel constructs (Movies S1-S2), nanowarming of cryoprotectant solution by MIH (Movie S3), convective warming of cryoprotectant solution (Movies S4-S5), cryomicroscopic study of NPs containing different cryoprotectant solution (Movies S6-S7), the viability of non-microencapsulated and microencapsulated pADSCs under different concentration of NPs and AC field (Tables S1-S2), cytotoxicity of Fe_3O_4 NPs at 4 °C (Figure S1), effect of nano-warming on non-encapsulated pADSCs after cryopreservation by low-CPA vitrification (Figure S2), morphology and viability of microencapsulated pADSCs after vitrification with different concentrations of Fe_3O_4 NPs and AC field (Figures S3-S5), and effect of nano-warming on the thermal profiles and cooling/warming rates during low-CPA vitrification (Figure S6).

The authors declare no competing financial interest.

combined use of alginate hydrogel microencapsulation and Fe3O4 nanoparticles-mediated nano-warming may be valuable to facilitate widespread application of stem cells in the clinic.

Table of contents (TOC)

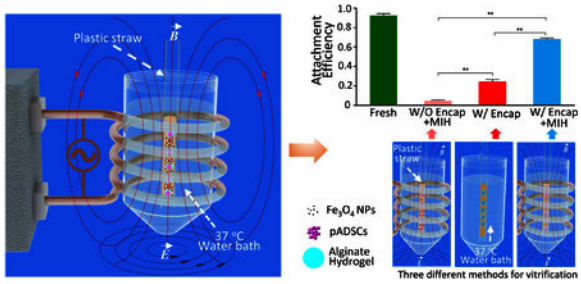

Keywords

stem cell-hydrogel constructs; nano-warming; magnetic induction heating; Fe_3O_4 nanoparticles; vitrification

INTRODUCTION

Recently, stem cell-alginate hydrogel constructs have attracted wide attention for various biomedical applications including 3D cell culture, cell delivery, cellular therapy, assisted reproduction, regenerative medicine and tissue engineering.[1–11] As with most extracellular matrices, hydrogel is mainly made of water and may be used to mimic the *in vivo* microenvironment for cell culture.[12] Moreover, it has been used to microencapsulate cells to protect them from being killed by host immune system *in vivo*, maintain them in the desired position in host, and to direct the differentiation of microencapsulated stem cells towards the desired lineages,[13–20] while allowing adequate diffusion of nutrients and metabolic wastes.[15, 21–22] However, the shelf-life of the cell-alginate hydrogel constructs at ambient temperature is very limited (days to weeks at most). Therefore, cryopreservation of the constructs to achieve long-term storage and banking for their wide ready availability is an enabling technology for their clinical applications. The cryopreservation of constructs must maintain not only the viability and function of encapsulated cells or tissues, but also the integrity of composite materials. These two aspects are at lease equally important for their further applications.[23]

The existing cryopreservation methods for cell-alginate hydrogel constructs include slow freezing and vitrification. The extensive ice formation associated with the slow freezing method, often causes microstructural damage to the hydrogel constructs, in addition to freeze-concentration induced cryoinjury to the cells in the constructs.[23–24] Furthermore, the process of slow freezing is time consuming and may require an expensive programmable freezer.[25–26] Vitrification cryopreservation is fast without the need of any special freezer, and constructs with intact microstructure can be obtained post-cryopreservation. However, achieving vitrification during cooling and suppressing devitrification during warming require high concentrations of cryoprotective agents (CPAs), up to ~6–8 M, which could

cause osmotic and metabolic injuries to the cells.[27–29] In addition, the multi-step loading/unloading of CPAs to reduce these injuries is time consuming, stressful, and complex to operate.[30] To address these problems, low-CPA vitrification is attracting increasing attention for the cryopreservation of cell-alginate hydrogel constructs. This is because it not only can prevent the damage to the construct microstructure and cells that occurs during slow freezing, but also avoid both osmotic and metabolic injuries to cells and the multi-step loading/unloading of CPAs associated with high-CPA vitrification. To achieve low-CPA vitrification, a commonly used strategy is to reduce the sample volume to a few microliters or less so that an ultra-rapid cooling/warming rates (>100,000 °C min^{-1}) could be achieved to suppress ice formation by minimizing the time for ice formation.[31–32] However, the small volume allowed by this strategy limits their practical application to cells (*e.g.*, oocytes) that exist in a small number.

Another strategy to achieve low-CPA vitrification is to slow down the rate of ice formation during cooling and warming so that an ultra-rapid cooling/warming is not necessary and large sample volume can be used. For example, recent studies have revealed that alginate hydrogel not only can preferentially promote the vitrification of water encapsulated in small alginate hydrogel microcapsules at low-CPA concentrations but also inhibit devitrification and recrystallization (lethal ice crystal formation during warming).[33] Therefore, alginate hydrogel is considered ideal for achieving low-CPA vitrification.[34]

Devitrification/recrystallization (devitification: ice formation in an ice crystal-free glass; recrystallization: the nucleation and/or growth of ice crystals) is a primary obstacle to successful vitrification of bio-samples. This is especially true for low-CPA vitrification. Recently, magnetic nanoparticles (NPs) have been added into the CPA solutions to increase the thermal conductivity of bio-samples and achieve enhanced and relatively uniform warming of cryopreserved bio-samples by selectively heating the NPs under an alternating magnetic field.[35–36] This approach may minimize devitrification/recrystallization by reducing the time for ice formation during warming (through increasing the warming rate), and possibly by directly suppressing ice formation and growth in the proximity of the selectively heated NPs that are distributed homogeneously in the CPA solution. However, cells in close proximity to the magnetic NPs may get overheated. In addition, studies have shown that high concentrations of magnetic NPs are potentially toxic to cells[37–41] and it is desired to avoid direct contact between the cells and magnetic NPs. Moreover, electromagnetic heating has not been explored for the warming of cryopreserved cell-alginate hydrogel constructs.

In this work, we developed a novel approach to successfully achieve the low-CPA (2 M penetrating CPAs) vitrification of stem cell-alginate hydrogel constructs (~500 μm in diameter) by combining nano-warming via magnetic induction heating (MIH) of Fe_3O_4 NPs with alginate hydrogel microencapsulation. The cell-alginate hydrogel construct with a cell-laden alginate hydrogel core and a pure alginate hydrogel shell containing no cells was used in this study. Unlike the cell-alginate hydrogel construct without a shell, no cells are exposed on the surface of the constructs with a pure alginate hydrogel shell and the cells are completely separated from Fe_3O_4 NPs to eliminate any potential cytotoxicity to the cells. We found that high-quality cell-alginate hydrogel constructs with intact microstructures can be

obtained after cryopreservation. When the cells were not microencapsulated, cell survival was low (< 27%) either with or without nano-warming. Although the encapsulated cells without nano-warming retained relatively high immediate survival (63.5%), their long-term viability (attachment efficiency) was only 24%. Importantly, MIH increased not only the immediate cell survival (from 63% to 82%) but also the long-term cell survival by almost three times (from 24% to 68%). Moreover, the survived stem cells retained their intact proliferation and functions for further biomedical applications.

EXPERIMENTAL SECTION

Chemicals and Reagents.

All chemicals were purchased from Sigma (St. Louis, MO, USA), unless specifically indicated otherwise.

Synthesis and Characterization of Fe_3O_4 NPs.

The Fe_3O_4 NPs were prepared by a chemical co-precipitation method using $FeCl_24H_2O$ and $FeCl_36H_2O$, as detailed elsewhere.[42] The Fe_3O_4 NPs were vacuum-dried at 30 °C for 12 h and either used immediately or stored in a 4 °C refrigerator until use. The morphology of the Fe_3O_4 NPs was examined by transmission electron microscopy (TEM, Hitachi, Ltd., Tokyo, Japan) with an accelerating voltage of 100 kV. A dynamic light scattering (DLS) instrument (DynaPro-MS800, Wyatt Technology, Santa Barbara, CA, USA) was used to evaluate the size distribution of the Fe_3O_4 NPs. The surface zeta potential of the Fe_3O_4 NPs was measured using a Zeta Sizer Nano ZS90 (Malvern Instruments Ltd., Malvern, UK) at room temperature. The magnetic property of Fe_3O_4 NPs was characterized using a vibrating sample magnetometer (VSM, Quantum Design, Inc., San Diego, CA, USA) at room temperature. The phase composition of the NPs was determined by X-ray diffraction (XRD, Philips X'-Pert PRO, Netherlands) using the Cu Kα wavelength (λ = 1.54060 Å), and the measurement was performed in the angle range 2θ = 10–90° at a rate of 2.5° min^{-1}.

Cell Culture.

The porcine adipose-derived stem cells (pADSCs) were obtained as a gift from Yunhai Zhang's laboratory and isolated as previously described.[43] The pADSCs were cultured in Dulbecco's modified Eagle medium/Ham's Nutrient Mixture F-12 (DME/F12) containing 10% fetal bovine serum (FBS) (v/v), 50 μg mL^{-1} vitamin C, 10 ng mL^{-1} basic fibroblast growth factor (bFGF, Pepro Tech, USA), and 2 mM GlutaMAXTM-100 × (Life Technologies, USA) in a 37 °C, 5% CO_2 humidified incubator. The medium was changed every 3–4 days till the cells reached ~80–90% confluency. The adherent cells were then washed once in PBS, and detached with 0.25% trypsin-EDTA (Gibco, USA), centrifuged for 5 min at 94 × g, and re-suspended for passaging or further experimental use.

Cytotoxicity of Fe_3O_4 NPs.

A Cell Counting Kit-8 (CCK-8) was used to evaluate cell viability to determine the cytotoxicity of Fe_3O_4 NPs. The pADSCs were seeded in 96-well plates (BD Biosciences NJ, USA) at a density of 1×10^5 cells mL^{-1} and incubated overnight. The cells were incubated with a medium containing 0.1, 0.5, or 1% (w/v) Fe_3O_4 NPs at 37 °C in a 5% CO_2

humidified incubator for 1, 2, 3, 4, or 6 hours at 4 °C for 0.5, 1, and 2 h. The pADSCs without NP treatment was used as control group. A total of 10 μL CCK-8 reagent were added per well, and the plate was incubated for 4 h at 37 °C in a 5% CO_2 humidified incubator. Absorbance was then measured at 450 nm using a Microplate Reader (Diagnostics Pasteur, Marne la Coquette, France). The cell viability was calculated as the ratio of the absorbance of different experimental groups to that of the control group at different time periods.

We further detected the toxicity of Fe_3O_4 NPs at 4 °C. The suspended pADSCs were incubated with different concentrations of Fe_3O_4 NPs at 4 °C for 0.5, 1, and 2 h. The viability of the pADSCs was assessed by using an acridine orange/ethidium bromide (AO/EB) Staining kit (KeyGen Biotech Co., Ltd., Nanjing, China), following the manufacturer's instructions. The live cells stained by AO (green) and the dead cells stained by EB (red) were counted under an inverted fluorescence microscope (Ti-U, Nikon, Japan). At least 500 cells were counted for calculating the cell viability. All experiments were conducted 3 times.

Fabrication of Microfluidic Device.

A tube-in-tube device consisting of three glass capillaries with different diameters (150, 300 and 500 μm in outer diameter) was fabricated for cell microencapsulation. The three capillaries were fixed relative to each other by using a hot melt glue. Finally, the tube-in-tube capillary was fixed on a rectangular glass plate (9 × 4.5 × 0.3 cm) for convenient operation and observation under microscope. In the co-flow geometry, the three fluids flow in the same direction.

Generation of pADSC-Hydrogel Construct by Microfluidic Devices.

Syringes, "tube-in-tube" structured capillaries, and all other accessories were carefully washed with 75% (v/v) alcohol and sterile saline, and further sterilized using UV light in a laminar flow hood for 30 min. To generate the pADSC-hydrogel constructs (microcapsules), 2% (w/v) sodium alginate with pADSCs as the inner core fluid (cell density of 7.2×10^6 cells mL^{-1}) were injected from inlet I1, 2% (w/v) sodium alginate was pumped into inlet I2 as the outer alginate fluid, and corn oil was injected into inlet I3 as the continuous phase. The outlet of the device was immersed in 0.15 M $CaCl_2$ solution to cause the alginate micro-droplet to gel and form calcium alginate hydrogel constructs. The microcapsules settled down at the bottom of the culture dish during crosslinking. As a result the corn oil in the top layer and the CaCl2 solution in the middle layer could be removed by pouring. After that, the constructs at the bottom of the dish were further washed with 0.9% NaCl solution twice to remove the corn oil. To achieve isotonic osmolality, 2% sodium alginate was dissolved in 0.25 M aqueous D-mannitol solution. To prevent cell damage due to pH excursion, all the solutions were buffered with 10 mM HEPES to maintain pH 7.2 and filtered with 0.22 μm pore-size filters before use. The solutions were pumped into inlets I1, I2 and I3 using High-Precision Programmable Syringe Pumps (WK-101P, Nanjing Anerke Electronics Technology Co. Ltd., China) at flow rates of 10 μL min^{-1}, 20 μL min^{-1} and 600 μL min^{-1}, respectively. The microcapsules were generated using the tube-in-tube capillary device at

room temperature and collected in 0.15 M $CaCl_2$ solution at 4 °C in sterile petri dishes (6 cm in diameter).

Magnetic Induction Heating System.

The whole system consisted of five parts, *i.e.*, a water tank for cooling, a pump for delivering water, a magnetic induction heating system equipped with a 6-turn, water-cooled copper coil (4.5 cm in diameter), a heat exchanger, and a 37 °C water bath.

Determination of the Thermal History during Cryopreservation.

The thermal history of the CPA solution was recorded using a fluorescence based fiber-optic temperature sensor (Indigo Precision Optoelectronics Technology Co., Ltd. Suzhou, China) during the cooling/warming processes. The sensor probe was fixed at the center of the plastic straw (PS), and 100 μL of a solution containing 1 M dimethyl sulfoxide (DMSO), 1 M ethylene glycol (EG) and 1.3 M trehalose was loaded either with or without 0.5% (w/v) Fe_3O_4 NPs. The temperature was recorded every 1 second during the cooling and warming processes.

SEM Imaging of Stem Cell-Alginate Hydrogel Constructs.

The cell-alginate hydrogel constructs (microcapsules) with 0.5% (w/v) Fe_3O_4 NPs were incubated overnight at 4 °C, before and after vitrification with nano-warming. Then, the constructs were freeze-dried using a Linkam FDCS196 cryostage (Linkam, Surrey, UK). The dried microcapsules were sputter-coated with gold, and their surface and internal textural were analyzed by scanning electron microscopy (SEM, JEOL Model JSM-6390 LA).

Alginate Hydrogel Prevents Cell Uptake of Fe_3O_4 NPs.

The 0.5% Fe_3O_4 NPs were dispersed in complete culture medium, and then incubated with pADSCs or pADSCs-hydrogel constructs for 10 h at 37 °C in a 5% CO_2 humidified incubator. Afterward, the constructs were dissolved in 75 mM sodium citrate for 2 min to release the encapsulated stem cells. The pADSCs were fixed with 2.5% (v/v) glutaraldehyde and prepared for examination using TEM.

Vitrification of pADSC-Hydrogel Constructs.

In this study, the CPA solution consisted of 1 M EG, 1 M DMSO, 1.3 M trehalose and in DME/F12 medium with 60% FBS. The non-encapsulated pADSCs or pADSC-hydrogel construct (encapsulated pADSCs) was incubated in medium containing 1 M EG and 1 M DMSO for 10 min and 20 min at 4 °C, respectively. Then, the penetrating CPAs were removed, and the cells were incubated in the CPAs with 0.1, 0.5, or 1% (w/v) Fe_3O_4 NPs for 10 min at 4 °C. Finally, the non-encapsulated or encapsulated pADSCs were transferred into a PS (FHK, Japan) as soon as possible. The PS was plunged into liquid nitrogen (LN2) and held for about 3 min to quire full thermal equilibrium.

Nano-Warming by MIH of Fe_3O_4 NPs.

The cryopreserved samples were warmed back to 37 °C by removing PS from the LN2 and plunging it into medium at 37 °C under an alternating current (AC) magnetic field generated by a 6-loop coil apparatus (Shenzhen Shuangping Power Supply Technology Co., Ltd., China) at a medium frequency (375 kHz) for 10 seconds. A portion of the constructs were dissolved in 75 mM sodium citrate for 2 min to release the encapsulated stem cells. The released stem cells were centrifuged at 94 × g for 5 min and resuspended in DME/F12 medium for further experiments or culture. The remaining portion of the constructs were cultured in 12-well plates for further experiments.

Assessment of Cell Viability, Attachment and Proliferation Post-Vitrification.

The immediate viability of the pADSCs was assessed using an AO/EB Staining Kit as aforementioned. To quantify attachment efficiency, fresh or post-cryopreservation pADSCs were seeded in 24-well plates, and on the second day, the attached and suspended cells were counted with the Muse™ Cell Analyzer (Merck Millipore, Germany) using a Cell Count and Viability Kit (Merck Millipore, Germany). The attachment efficiency was defined as the percentage of attached cells out of the total number of cells (*i.e.*, attached and suspended cells). To quantify the pADSC proliferation, fresh and cryopreserved cells were seeded in 96-well plates at a density of 1×10^4 cells mL^{-1} for culturing. After 1, 2, and 3 d, 10 μL CCK-8 reagent was added in each well, and the 96-well plates were placed at 37 °C in a 5% CO_2 humidified incubator. After 4 h, the absorbance of each well was measured at 450 nm using a plate reader. The cell proliferation was assessed as the ratio of the absorbance on day 2 and day 3 to that on day 1.

Functional Testing of pADSCs.

To further study the effect of pADSC vitrification, fresh and cryopreserved stem cells were seeded at a density of 1×10^4 cells cm^{-2} in 25 cm^2 plastic culture flasks (Corning Incorporated, NY, USA). When the cells reached ~90% confluence, they were detached for further experiments. First, immunofluorescent staining for three surface markers CD44+, CD29+, and $CD31^-$, was performed according to the standard immunofluorescent methods.[44] The samples were further stained for nuclei using 4', 6-diamidino-2-phenylindole (DAPI, Beyotime, Haimen, China) at room temperature for 10 min. The samples were then washed with PBS, mounted using a few drops of Antifade Mounting Medium (Beyotime, Haimen, China), and imaged using an inverted fluorescence microscope (Nikon Eclipse Ti-U, Tokyo, Japan).

The expression of the CD44+, CD29+, CD90+, and $CD31^-$ surface markers was further analyzed by flow cytometry (FCM), for which the pADSCs were detached with trypsin/EDTA, washed three times (5 min each time) with PBS, and stained with the primary antibodies CD44-FITC (1:1000 dilution, Invitrogen, USA), CD31-FITC (1:500 dilution, Abcam, USA), CD29-FITC (1:500 dilution, BD Pharmingen, USA) and CD90-FITC (1:500 dilution, BD Pharmingen, USA) at 4 °C for 1.5 h. The stained samples were washed three times with PBS to remove the free secondary antibody and analyzed using a flow cytometer (BD FACSVerse™, New Jersey, USA) together with the FACS suite software.

Finally, the multi-lineage potential of pADSCs was tested by adipogenic and osteogenic differentiation. The pADSCs were detached with trypsin/EDTA and further cultured in 12-well plates till the cells reached ~60–80% confluency. Then, the culture medium was removed, and adipogenic or osteogenic differentiation medium (Thermo Scientific, USA) was added to culture for 14 d and 21 d, respectively. On the last day of differentiation experiment, after the differentiation medium was removed, the differentiated cells were washed with 1 × PBS three times, fixed with 4% paraformaldehyde for 30 min at room temperature, and rinsed three times with 1 × PBS. The samples for adipogenic differentiation were stained with Oil Red O for 60 min, and the cell nucleus was stained with DAPI. Osteogenesis was confirmed by staining with Alizarin Red S stain for 10 min. The stained cells were examined under an inverted fluorescence microscope (Nikon Eclipse Ti-U, Nikon, Japan).

Viability and Proliferation of Stem Cells in Constructs Post-Vitrification.

The cell-alginate hydrogel constructs post-vitrification were cultured in 12-well plates for 0, 3 and 7 days to study the viability and proliferation of the cells in the constructs.

Cryomicroscopy Study of Fe_3O_4 NPs and Alginate Hydrogel.

To further understand the role of NPs and hydrogels in cryopreservation, a Linkam FDCS196 cryostage was used for cryomicroscopic studies of Fe3O4 NPs and alginate hydrogel. Experimental samples with a thickness of 200 μm, including CPA (1M EG, 1M DMSO and 1.3 M trehalose), CPA with Fe_3O_4 NPs, and CPA with alginate hydrogel, were cooled at 10 °C/min from 25 °C to −4 °C, held for 2 min, cooled at 100 °C/min to −120 °C, held for 3 min, and warmed at 100 °C/min to room temperature.

Statistical Analysis.

All data are presented as mean ± standard deviation (SD) of results from at least four independent runs. The statistical difference was determined using a two-tailed unpaired Student's *t-test* or one-way analysis of variance. A p value less than 0.05 was considered as statistically significant.

RESULTS AND DISCUSSION

Characterization and Cytotoxicity of Fe_3O_4 NPs.

The morphology of the Fe_3O_4 NPs was characterized using TEM, as shown in Figure 1A. All the NPs are nearly spherical and uniform in size (16.5 ± 3.0 nm in diameter). The size distribution of the Fe_3O_4 NPs is shown in Figure 1B, and the average hydrodynamic diameter of the NPs was found by DLS to be 25.5 ± 2.7 nm. The hydrodynamic diameter is slightly larger than that observed by TEM because the NPs associate easily with water molecules and are prone to form a hydrated layer on their surface.[36] As shown in Figure 1C, the NPs have a negatively charged surface (−21.8 ± 4.0 mV) in deionized water (pH = 7.4) at room temperature. The magnetization curve of the NPs is shown in Figure 1D, and indicates a saturation magnetization of 65 emu g^{-1}, which is consistent with previous studies.[42] The NPs exhibit good magnetic responsiveness under a magnetic field (inset of Figure 1D). Figure 1E shows the XRD pattern of the Fe_3O_4 NPs, which matches well with the standard

diffraction pattern of Fe_3O_4 (JCPDS card No.82–1533),[42] and no characteristic impurity peaks are observable. Therefore, the NPs consist solely of Fe_3O_4 without impurities.

The cytotoxicity of Fe_3O_4 NPs was evaluated by CCK-8 assay at 37 °C and 4 °C, as shown in Figure 1F and G, respectively. For the vitrification experiments, the cell suspension with NPs was kept below 4 °C for less than 2 hours. Therefore, we only evaluated the cytotoxicity of NPs at 4 °C for 2 hours. The results show that Fe_3 O_4 NPs exhibit both time-dependent and concentration-dependent cytotoxicity when the cells were cultured with different concentrations (0.1, 0.5, and 1% (w/v)) of Fe_3O_4 NPs at 37 °C for 1 to 6 h (Figure 1F). However, no obvious cytotoxic effects on the cells treated with different concentrations (0.1, 0.5, and 1% (w/v)) of Fe_3O_4 NPs at 4 °C for 0.5, 1, and 2 h were observed (Figure 1G). The viability of cells with different concentrations of NPs was measured further by AO/EB double staining at 4 °C for 0.5, 1, and 2 h, as shown in Figure S1 (Supporting Information). The results show that the NPs had no significant cytotoxicity at 4 °C, which is consistent with the results of the aforementioned CCK-8 tests. The cytotoxicity of the Fe_3O_4 NPs increased with increasing temperature. Since the cell metabolism is more active at high temperature (e.g., 37 °C) than at low temperature (e.g., 4 °C), the NPs are more likely to enter the cells at 37 °C. However, a high intracellular concentration of NPs could induce the generation of undesired free radicals, which could cause cell membrane damage, oxidative DNA lesions and cytoskeleton injuries.[45–46] In addition, NP internalization could cause some cells to generate auto-phagosomes, which can cause changes in cell morphology and result in programmed cell death.[47–48]

Generation of pADSC-Alginate Hydrogel Constructs.

The tube-in-tube capillary microfluidic device for generating pADSC-alginate hydrogel constructs, the configuration of the tube-in-tube capillary, and the vitrification procedure with warming in 37 °C water bath are illustrated in Figure 2A and Movie S1 (Supporting Information). The device consists of an inner capillary (for flowing 2% sodium alginate and cells), a middle capillary (for flowing 2% alginate), and an outer capillary (for flowing corn oil) connected to the three inlets, I1, I2 and I3, respectively. The specific dimensions of the three glass capillaries are shown in inset (i) of Figure 2A. Due to shear stress and interfacial tension, the inner flow of cell-sodium alginate mixture and the middle flow of pure sodium alginate are dispersed into microdroplets by the outer oil flow. The microdroplets suspended in oil are further gelled into alginate hydrogel. The sodium alginate/alginate hydrogel shell can protect the encapsulated cells from external environmental damage during their generation (*e.g.*, shear stress damage)[49] and further applications (e.g., shear stress during injection and immune rejection after transplantation).[50–51] The size of the alginate hydrogel constructs (*i.e.*, microcapsules) can be controlled by adjusting the flow rates of the three different flows. When the inner, middle, and outer flow rates are set as 10, 20 and 600 μL min^{-1}, respectively, the resultant microcapsules are 521.8 ± 25.5 μm in diameter, as shown in Figure 2B and C. Two factors may suppress the mixing between the core and the shell flows, and to form core-shell structured microcapsules, i.e., i) laminar flows in the glass capillaries, and ii) the significantly enhanced viscosity of the solutions by 2% sodium alginate. This is confirmed by the micrographs of the generated microcapsules shown in Figure 2B. At these flow rates, the device could generate approximately 100 microcapsules

per minute (as shown in Movie S2), and the cell encapsulation rate is approximately 500 cells s^{-1}. This is 10 times higher than that previously reported (50 cells s^{-1}).[52] The cell concentration could be further increased to shorten the generation time and enhance the throughput.

Nano-Warming by MIH of Fe_3O_4 NPs.

It has been reported that solution containing Fe_3O_4 NPs can be rapidly and uniformly heated under an AC magnetic field.[36, 53] According to this characteristic, in this study, the Fe_3O_4 NPs were introduced into the warming process of cryopreservation of bio-samples. As shown in Figure 3A, the CPA solution (1 M DMSO, 1 M EG, and 1.3 M trehalose) with NPs (Plastic straw #1, PS #1) and without NPs (PS #3) was vitrified and there was no obvious change in appearance. In contrast, the culture medium with NPs (PS #2) and without NPs (PS #4) was frozen (*i.e.*, formed ice): the transparent and darkish samples without or with NPs became opaque or whitish after cooling.

A schematic illustration of nano-warming *via* MIH of NPs was shown in Figure 3B. A 0.25-mL PS containing cell-alginate hydrogel constructs and NPs in CPA solution was plunged into a centrifuge tube with 37 °C water in an inductive 6-turn coil. The process of nano-warming is further demonstrated in Figure 3C (a1-c1) and Movie S3. For comparison, the processes of conventional warming in 37 °C water bath (with or without Fe3O4 NPs) are demonstrated in Figure 3C (a2-c2 and a3-c3) and Movies S4–5. The results show that devitrification/recrystallization occurred during both nano-warming and conventional warming. During nano-warming or conventional warming, sample containing CPA solution (with or without 1% (w/v) Fe3O4 NPs) forms ice. If the time when devitrification/recrystallization started was set as 0 s, devitrification/recrystallization ended at 0.36, 0.38, and 0.56 s and ice crystals melted completely at 1.84, 2.48, and 3.2 s for nano-warming (15 A), and conventional warming with and without NPs, respectively. Due to the low thermal conductivity of the bio-sample, it is extremely difficult (if not impossible) to achieve a sufficient warming rate to prevent devitrification/recrystallization with 37 °C water-bath alone. Therefore, when Fe_3O_4 NPs were added to the CPA solution, more rapid and uniform warming of the cryopreserved bio-sample could be achieved under an AC magnetic field. Moreover, the NPs could be used as a homogeneously distributed heat sources to reduce ice formation and growth (*i.e.*, devitrification and ice recrystallization) in their proximity during nano-warming.

Morphology of Cell-Alginate Hydrogel Constructs and Cell Uptake of Fe_3O_4 NPs.

The morphology of the cell-alginate hydrogel constructs was analyzed by SEM under three conditions: before and after vitrification of the constructs with nano-warming, and after incubating the constructs (cell-laden microcapsules) with Fe3O4 NPs overnight at 4 °C. As shown in Figure 4A, the morphology of the cell-alginate hydrogel construct post-vitrification is similar to that of the constructs before vitrification. Unlike slow freezing that could cause damage to the microcapsule microstructure,[25, 34] an intact microstructure can be maintained with the proposed vitrification approach. This is desired for further applying the constructs for cellular therapies and regenerative medicine. In Figure 4A (bottom row), the Fe_3O_4 NPs appear only on the surface of the microcapsules. When non-encapsulated

pADSCs and pADSCs-hydrogel constructs (encapsulated pADSCs) were incubated with Fe_3O_4 NPs for 10 h at 37 °C, the NPs could be observed in non-encapsulated cells (Figure 4B (a)) while no NPs were found in the encapsulated cells (Figure 4B (b)). The results indicate that the alginate hydrogel shell could keep the NPs outside the microcapsules and separate the microencapsulated cells from the NPs, to minimize the potential cytotoxicity of the NPs.

Cell Viability, Attachment Efficiency, and Proliferation Post-Vitrification.

PS has been widely used for cell cryopreservation by vitrification with high concentration of penetrating CPAs. To reduce the cytotoxicity of the penetrating CPAs (at high concentration) and to achieve vitrification, 1.3 M trehalose, a non-penetrating CPA, was added to the CPA solution containing 1 M DMSO and 1 M EG in this study.

Figure 5A and Table S1 (Supporting Information) show the viability of non-microencapsulated cells under different conditions: fresh, CPA treating or post-vitrification without NPs and with 0.1, 0.5, or 1% (w/v) NPs with nano-warming by MIH under an AC magnetic field (5A, 15A and 25A). Due to the low concentration of CPAs used, the non-encapsulated cell viability post-vitrification is low (< 30%) although the cell viability could be slightly improved with MIH probably by reducing ice formation during warming. Compared with fresh cells, many of the non-encapsulated pADSCs post-vitrification are ruptured and dead, as shown in Figure S2. This may be because recrystallization or devitrification induced injury is lethal to cells during warming,[54–55] although vitrification could decrease cell injury during cooling. The Fe3O4 NPs are used as homogeneously distributed heat sources to reduce ice formation during nano-warming, but a high concentration of NPs may generate instantaneous overheating of cells immediately next to the NPs to kills the cells.

It has been reported that the water in alginate hydrogel microcapsules can be preferentially vitrified over the water outside the microcapsule during cooling, and alginate hydrogel can reduce devitrification and recrystallization during the warming process.[52] Therefore, the pADSCs are microencapsulated in alginate hydrogel to form cell-alginate hydrogel constructs for cryopreservation by low-CPA vitrification. To exclude the effect of the loading/unloading of CPAs, the cell viability was examined after the two-step loading/unloading of CPAs, and the results show (Figure 5A-B) that this approach to CPA treatment has little effect on cell viability. Indeed, as shown in Figure 5B and Table S2, the viability of the microencapsulated cells post-vitrification without nano-warming (No NPs) is approximately 63.5%, which is much and significantly higher than that of the non-microencapsulated cells post vitrification under the same condition. However, the viability is less than 70%, which is the lowest acceptable cell viability for cell therapy according to the FDA guidelines.[56] To further enhance the cell viability post vitrification, nano-warming *via* the MIH of Fe_3O_4 NPs was performed. To obtain optimal MIH conditions for nano-warming, the effect of the current intensity and concentration of Fe_3O_4 NPs on the cell viability was investigated. When 0.1% (w/v) NPs is added, the viability of the microencapsulated pADSCs post-vitrification does not increase significantly as the current intensity is varied from 5 to 25 A. This is probably because too low a concentration of NPs

does not allow MIH to produce enough heat to reduce the nucleation and growth of lethal extracellular and intracellular ice crystals during warming. When the concentration of NPs is increased to 0.5% (w/v), the NPs could serve as extensive and uniformly distributed heating sources, which could generate heat to reduce extracellular and intracellular ice nucleation and growth during warming. However, when the concentration of NPs is increased to 1% (w/v), the viability is not significantly improved compared with that at 0.5% (w/v). Collectively, the data show that the viability of microencapsulated pADSCs post-vitrification is the highest (~82.3%) in a CPA solution with 0.5% (w/v) Fe_3O_4 NPs at 15 A. Figure 5C shows representative DIC and live/dead (green/red) stain images of pADSCs in microcapsules under different conditions, *i.e.*, fresh, post-vitrification without NPs, and post-vitrification with 0.5% (w/v) NPs heated by MIH under an AC magnetic field (15 A). The morphology and live/dead stain of pADSCs after releasing out of the microcapsules under these three conditions are shown in Figure 5D. The morphology of pADSCs after vitrification by nano-warming is similar to that of fresh cells. Typical DIC and fluorescence images showing the morphology and viability of pADSCs under the other conditions are shown in Figures S3–5.

To further assess the long-term cell viability post-vitrification, the attachment efficiency and proliferation of pADSCs were studied after vitrification cryopreservation. As shown in Figure 5E, the attachment efficiency of pADSCs after nano-warming is 68.2%, which is much higher than that (24.1%) of cells subjected to conventional warming in 37 °C water bath alone. Under the same conditions with nano-warming, the attachment efficiency is only 4.1% if the cells are not microencapsulated. The proliferation of fresh and post-vitrification pADSCs (after both conventional and nano-warming by MIH) are shown in Figure 5F. No significant differences are observed between the two groups. Representative images showing the attachment and proliferation of pADSCs under various conditions are presented in Figure 5G and H, respectively. Although the viability of encapsulated cells subjected to conventional warming is relatively high (63.5%), the attachment efficiency is very low (24.3%). This indicates that many cells with intact membranes could not attach, probably because they are under apoptosis.[35, 57] After cryopreservation, the gene expression of adhesion-related molecules may be downregulated, which reduces cell attachment efficiency.[58] The attachment efficiency of vitrified cells in constructs subjected to nano-warming is significantly improved, possibly because the nano-warming by MIH could minimize devitrification or recrystallization-induced injury so that the pathways for apoptosis and degradation of adhesion proteins were not triggered by vitrification. The ability of cryopreserved cells to attach is very important for their further applications.

Functional Properties of pADSCs Post-Vitrification with Nano-Warming.

To further study the functional survival of the pADSCs post-vitrification with nano-warming by MIH of 0.5% (w/v) Fe_3O_4 NPs (15 A), the sternness and capability of multi-lineage differentiation of the pADSCs were investigated. Typical pADSC markers including CD44, CD29, CD90, and the negative marker CD31 were analyzed by immunostaining and flow cytometry.[59–60] As shown in Figure 6A and B, CD44, CD29, and CD90 are expressed on both fresh pADSCs and microencapsulated cells post-vitrification with nano-warming, and there is no evident difference between the fresh and vitrified groups. Moreover, the

expression of CD31 is low in both groups. The sternness of pADSCs was further studied by characterizing their capability of adipogenic and osteogenic differentiation (Figure 6C). Both the fresh and post-vitrification pADSCs show similar potential for adipogenic and osteogenic differentiation. The results indicate that microencapsulated pADSCs post-vitrification with nano-warming by MIH retain their specific functional properties, which is very important for the application of cell-alginate hydrogel constructs.

3D Culture of the Constructs Post-Vitrification.

To demonstrate the suitability for further applications of cell-alginate hydrogel constructs post vitrification, the long-term viability/proliferation of cells in the constructs post-vitrification were examined. As shown in Figure 7, high cell viability is achieved in the fresh group and in the constructs post-vitrification on days 0, 3, and 7 under 3D culture. The proliferation of the pADSCs in constructs post-vitrification is similar to that of the fresh group. The results indicate that cells could maintain high long-term viability after vitrification with nano-warming. The cells in the constructs were observed to form many small cell aggregates on day 7 in both the fresh and vitrified groups. The results further support that cells could maintain high long-term viability in cell-alginate hydrogel constructs after vitrification with nano-warming, which is important for further biomedical applications of the constructs (e.g., implantation, drug screening, *etc.*).

Cryomicroscopic Analysis and Possible Mechanism of Nano-Warming by MIH.

Cryomicroscopy studies of Fe3O4 NPs and alginate hydrogel were performed using a Linkam FDCS196 cryostage to understand the role of NPs and hydrogels played in cryopreservation, as illustrated in Figure 8A. The cryomicroscopic results were shown in Figure 8B and Movies S6–8. When the sample containing CPA solution with a thickness of 200 μm was cooled at 100 °C/min, ice crystals appeared at −70.8 °C and continued to grow till −94.2 °C and during warming at 100 °C/min, recrystallization occurred at −19.7 °C. Correspondingly, when 0.05% (w/v) Fe_3O_4 NPs were added to the CPA solution for cooling and warming at the 100 °C/min, ice crystals formed at −61.9 °C and continued to grow till −70.6 °C during cooling, and during warming, recrystallization occurred at −20.6 °C. Nevertheless, if the alginate hydrogel with a thickness of 200 μm was soaked in CPA solution for 2 h for cooling at 100 °C/min, ice crystals did not appear until −84.1 °C. Compared with aforementioned two groups, the ice crystals in the alginate hydrogels were smaller in size and less in quantity. Importantly, recrystallization did not occur during warming. These results suggested that the NPs decreased the undercooling of CPA solution and promoted the formation of ice crystals during cooling, and alginate hydrogel could decrease and/or inhibit ice formation during cooling and warming. The reduction of undercooling is advantageous for cryopreservation of bio-samples.[61]

To further study the effect of nano-warming on vitrification, the thermal history of the CPA solution (including 1 M EG, 1 M DMSO and 1.3 M trehalose with or without 0.5% (w/v) NPs) was recorded throughout the cooling-warming process, and the cooling and warming rates were calculated as the rate of temperature change over time. As shown in Figure S6, with nano-warming, the temperature changes more rapidly during the initial stage of warming.as may be attributed to the spatial heating of NPs in the alternating magnetic field;

while the introduction of NPs seems not to obviously affect the cooling rate. The smooth thermal history indicate that there was no appreciable latent heat release during the cooling process, suggest that the CPA solution underwent glass transition during cooling.[62] Overall, the temperature in the sample with nano-warming was increased, probably due to the improved warming rate during the first few seconds under an AC magnetic field.

It has been reported that there is a dangerous temperature zone (from approximately −10 to −30 °C, which may be different for different CPA solutions) during warming cryopreserved samples when recrystallization and/or devitrification tend to occur.[52, 63] The possible mechanism of nano-warming in improving the outcome of cell cryopreservation by vitrification is proposed and schematically illustrated in Figure 8C. When NPs are present in the CPA solution, they can serve as numerous heating sources under an AC magnetic field and produce heat to suppress the nucleation and growth of lethal ice crystals during warming locally in their proximity and globally during warming across the dangerous temperature zone. This minimizes devitrification and recrystallization induced damage to cells. The sample can also pass through the dangerous temperature zone more rapidly during nano-warming with shortened time (Figure 3) for possible detrimental effect of devitrification and/or recrystallization to occur.

During the cooling process, invisible small intercellular ice crystals might form in many of the non-encapsulated cells and could grow to form large ice crystals during conventional warming, which could cause mechanical damage and possible apoptosis to cells. Although Fe_3O_4 NPs could be used as homogeneously distributed heat sources to suppress ice formation during the nano-warming process, the high-concentration NPs that are in direct contact with the cells could produce localized overheating that could result in cell death. Moreover, small intercellular cell ice crystals formed in many of the non-encapsulated cells could grow and form large lethal ice crystals during nano-warming to kill the cells.

The alginate hydrogel not only can promote vitrification of CPA solution during cooling, but also inhibit devitrification/recrystallization during warming.[33, 52] Therefore, extracellular ice formation (in the hydrogel) will be significantly suppressed for the cells encapsulated in alginate hydrogel microcapsules during both cooling and warming. As a result, the damage to the cells after warming is reduced and cell viability is improved. However, the viability of cells in large (> 250 μm in diameter) cell-alginate hydrogel constructs was not very high (63.5%) after vitrification with conventional warming. Furthermore, many of the cells that are viable judged by live/dead staining could not attach, possibly because of apoptosis or downregulation of the expression of adhesion proteins.[57–58] This issue could be overcome by nano-warming to both locally and globally minimize devitrification and recrystallization induced cell injury. Moreover, the alginate hydrogel shell of the microcapsules could prevent direct contact between the cells and NPs, which could minimize the potential cytotoxicity of the high-concentration of NPs, localized overheating of cells, and mechanical damage by large ice crystals outside the constructs during nano-warming by MIH. Furthermore, no damage to the microstructure would occur during vitrification. Therefore, intact cell-alginate hydrogel constructs with high cell viability could be obtained using nano-warming by the MIH of Fe_3O_4 NPs.

CONCLUSIONS

In this study, we successfully achieved low-CPA vitrification of stem cell-alginate hydrogel constructs by combining nano-warming with MIH of Fe_3O_4 NPs and microencapsulation with alginate hydrogel. The hydrogel shell of the constructs could protect encapsulated cells from damage caused by large ice crystals outside the constructs during cryopreservation and could separate the encapsulated cells from high concentrations of Fe_3O_4 NPs. The alginate hydrogel could enhance vitrification during cooling and suppress devitrification/recrystallization during warming. At the same time, the NPs could be used as a homogeneously distributed heating source to further suppress devitrification and recrystallization both locally and globally during warming under an AC magnetic field. With this approach, high-quality cell-alginate hydrogel constructs with intact microstructure and high cell survival can be obtained after low-CPA vitrification. Importantly, compared with conventional warming, nano-warming could increase the long-term survival (attachment efficiency) of cells in the cell-alginate hydrogel constructs by nearly three times (from 24% to 68%). Moreover, the cells in the cell-alginate hydrogel construct post vitrification retain their intact functional properties with high survival under long-term 3D culture. This novel low-CPA vitrification approach may be valuable for facilitating the widespread application of the cell-alginate hydrogel constructs in the field of cell-based medicine.

Supplementary Material

Refer to Web version on PubMed Central for supplementary material.

ACKNOWLEDGMENTS

This work was supported by the National Natural Science Foundation of China (No. 51476160 to G Z.) and the U.S. National Institutes of Health (grants R01EB012108 and R01EB023632 to X.H.). This work was partially performed at the USTC Center for Micro- and Nano-scale Research and Fabrication.

REFERENCES

(1)Guilak Farshid, Cohen Daniel, M., Estes Bradley, T., Gimble Jeffrey, M., Liedtke Wolfgang.. Control of Stem Cell Fate by Physical Interactions with the Extracellular Matrix Cell Stem Cell. 2009; 5(1):17–26. [PubMed: 19570510]

(2)Perez RA, Kim M, Kim TH, Kim JH, Lee JH, Park JH, Knowles JC, Kim HW. Utilizing core-shell fibrous collagen-alginate hydrogel cell delivery system for bone tissue engineering Tissue Eng Pt A. 2014; 20(1–2):103–114.

(3)Ballios BG, Cooke MJ, Donaldson L, Coles BL, Morshead CM, Van d. K. D., Shoichet MS. A Hyaluronan-Based Injectable Hydrogel Improves the Survival and Integration of Stem Cell Progeny following Transplantation Stem Cell Rep. 2015; 4(6):1031–1045.

(4)Xu M, Banc A, Woodruff TK, Shea LD. Secondary follicle growth and oocyte maturation by culture in alginate hydrogel following cryopreservation of the ovary or individual follicles Biotechnology & Bioengineering. 2009; 103(2):378–386. [PubMed: 19191350]

(5)Zhao S, Xu Z, Wang H, Reese BE, Gushchina LV, Jiang M, Agarwal P, Xu J, Zhang M, Shen R. Bioengineering of injectable encapsulated aggregates of pluripotent stem cells for therapy of myocardial infarction Nat Commun. 2016; 7:13306. [PubMed: 27786170]

(6)Jordan AM, Kim SE, Voorde KVD, Pokorski JK, Korley LSTJ. In Situ Fabrication of Fiber Reinforced Three-Dimensional Hydrogel Tissue Engineering Scaffolds Acs Biomaterials Science & Engineering. 2017; 3(8):1869–1879.

(7)Rodrigues GM, Gaj T, Adil MM, Wahba J, Rao AT, Lorbeer FK, Kulkarni RU, Diogo MM, Cabral JM, Miller EW. Defined and scalable differentiation of human oligodendrocyte precursors from pluripotent stem cells in a 3D culture system Stem Cell Rep. 2017; 8(6):1770–1783.

(8)Wang X, Zhang J, Cui W, Fang Y, Li L, Ji S, Mao D, Ke T, Yao X, Ding D. Composite hydrogel modified by IGF-1C domain improves stem cell therapy for limb ischemia ACS applied materials & interfaces. 2018; 10(5):4481–4493. [PubMed: 29327586]

(9)Qi J, Yan Y, Cheng B, Deng L, Shao Z-W, Sun Z, Li X. Enzymatic Formation of an Injectable Hydrogel from a Glycopeptide as a Biomimetic Scaffold for Vascularization ACS applied materials & interfaces. 2018; 10(7):6180–6189. [PubMed: 29380599]

(10)Wang H, Cui J, Zheng Z, Shi Q, Sun T, Liu X, Huang Q, Fukuda T. Assembly of RGD-Modified Hydrogel Micromodules into Permeable Three-Dimensional Hollow Microtissues Mimicking in Vivo Tissue Structures ACS applied materials & interfaces. 2017; 9:41669–41679. [PubMed: 29130303]

(11)Li F, Truong VX, Thissen H, Frith JE, Forsythe JS. Microfluidic encapsulation of human mesenchymal stem cells for articular cartilage tissue regeneration ACS applied materials & interfaces. 2017; 9(10):8589–8601. [PubMed: 28225583]

(12)Ballios BG, Cooke MJ, Donaldson L, Coles BL, Morshead CM, van der Kooy D, Shoichet MS. A hyaluronan-based injectable hydrogel improves the survival and integration of stem cell progeny following transplantation Stem Cell Rep. 2015; 4(6):1031–1045.

(13)Burdick JA, Mauck RL, Gerecht S. To serve and protect: hydrogels to improve stem cell-based therapies Cell stem cell. 2016; 18(1):13–15. [PubMed: 26748751]

(14)Rowley JA, Madlambayan G, Mooney DJ. Alginate hydrogels as synthetic extracellular matrix materials Biomaterials. 1999; 20(1):45–53. [PubMed: 9916770]

(15)Chayosumrit M, Tuch B, Sidhu K. Alginate microcapsule for propagation and directed differentiation of hESCs to definitive endoderm Biomaterials. 2010; 31(3):505–514. [PubMed: 19833385]

(16)Ballios BG, Cooke MJ, van der Kooy D, Shoichet MS. A hydrogel-based stem cell delivery system to treat retinal degenerative diseases Biomaterials. 2010; 31(9):2555–2564. [PubMed: 20056272]

(17)Jacobs-Tulleneers-Thevissen D, Chintinne M, Ling Z, Gillard P, Schoonjans L, Delvaux G, Strand BL, Gorus F, Keymeulen B, Pipeleers D. Sustained function of alginate-encapsulated human islet cell implants in the peritoneal cavity of mice leading to a pilot study in a type 1 diabetic patient Diabetologia. 2013; 56(7):1605–1614. [PubMed: 23620058]

(18)Orive G, Hernandez RM, Gascón AR, Calafiore R, Chang TM, De Vos P, Hortelano G, Hunkeler D, Lacík I, Shapiro AJ. Cell encapsulation: promise and progress Nature medicine. 2003; 9(1): 104–107.

(19)Speranskaya ES, Sevrin C, De Saeger S, Hens Z, Goryacheva IY, Grandfils C. Synthesis of hydrophilic CuInS2/ZnS quantum dots with different polymeric shells and study of their cytotoxicity and hemocompatibility ACS applied materials & interfaces. 2016; 8(12):7613–7622. [PubMed: 26963807]

(20)Xu Q, He C, Zhang Z, Ren K, Chen X. Injectable, Biomolecule-Responsive Polypeptide Hydrogels for Cell Encapsulation and Facile Cell Recovery through Triggered Degradation ACS applied materials & interfaces. 2016; 8(45):30692–30702. [PubMed: 27762560]

(21)Kang A, Park J, Ju J, Jeong GS, Lee S-H. Cell encapsulation via microtechnologies Biomaterials. 2014; 35(9):2651–2663. [PubMed: 24439405]

(22)Murua A, Portero A, Orive G, Hernandez RM, de Castro M, Pedraz JL. Cell microencapsulation technology: towards clinical application J Control Release. 2008; 132(2):76–83. [PubMed: 18789985]

(23)Murua A, Orive G, Hernandez RM, Pedraz JL. Cryopreservation based on freezing protocols for the long-term storage of microencapsulated myoblasts Biomaterials. 2009; 30(20):3495–3501. [PubMed: 19327822]

(24)Gurruchaga H, Ciriza J, Del Burgo LS, Rodriguez-Madoz JR, Santos E, Prosper F, Hernandez RM, Orive G, Pedraz JL. Cryopreservation of microencapsulated murine mesenchymal stem cells genetically engineered to secrete erythropoietin International journal of pharmaceutics. 2015; 485(1):15–24. [PubMed: 25708005]

(25)Heng B, Yu Y-J, Ng S. Slow-cooling protocols for microcapsule cryopreservation Journal of microencapsulation. 2004; 21(4):455–467. [PubMed: 15513751]

(26)Duty SM, Singh NP, Ryan L, Chen Z, Lewis C, Huang T, Hauser R. Reliability of the comet assay in cryopreserved human sperm Human Reproduction. 2002; 17(5):1274–1280. [PubMed: 11980751]

(27)Agudelo CA, Iwata H. The development of alternative vitrification solutions for microencapsulated islets Biomaterials. 2008; 29(9):1167–1176. [PubMed: 18086496]

(28)Rall WF, Fahy GM. Ice-free cryopreservation of mouse embryos at −196 degrees C by vitrification Nature. 1985; 313(6003):573. [PubMed: 3969158]

(29)Yang J, Pan C, Zhang J, Sui X, Zhu Y, Wen C, Zhang L. Exploring the Potential of Biocompatible Osmoprotectants as Highly Efficient Cryoprotectants ACS applied materials & interfaces. 2017; 9(49):42516–42524. [PubMed: 29161015]

(30)Karlsson JO, Toner M. Long-term storage of tissues by cryopreservation: critical issues Biomaterials. 1996; 17(3):243–256. [PubMed: 8745321]

(31)He X, Park EY, Fowler A, Yarmush ML, Toner M. Vitrification by ultra-fast cooling at a low concentration of cryoprotectants in a quartz micro-capillary: a study using murine embryonic stem cells Cryobiology. 2008; 56(3):223–232. [PubMed: 18462712]

(32)Choi JK, Yue T, Huang H, Zhao G, Zhang M, He X. The crucial role of zona pellucida in cryopreservation of oocytes by vitrification Cryobiology. 2015; 71(2):350–355. [PubMed: 26297946]

(33)Zhang W, Yang G, Zhang A, Xu LX, He X. Preferential vitrification of water in small alginate microcapsules significantly augments cell cryopreservation by vitrification Biomedical Microdevices. 2010; 12(1):89–96. [PubMed: 19787454]

(34)Murua A, Orive G, Hernandez RM, Pedraz JL. Cryopreservation based on freezing protocols for the long-term storage of microencapsulated myoblasts Biomaterials. 2009; 30(20):3495–3501. [PubMed: 19327822]

(35)Wang J, Zhao G, Zhang Z, Xu X, He X. Magnetic induction heating of superparamagnetic nanoparticles during rewarming augments the recovery of hUCM-MSCs cryopreserved by vitrification Acta Biomater. 2016; 33:264–274. [PubMed: 26802443]

(36)Manuchehrabadi N, Gao Z, Zhang J, Ring HL, Shao Q, Liu F, McDermott M, Fok A, Rabin Y, Brockbank KG. Improved tissue cryopreservation using inductive heating of magnetic nanoparticles Science translational medicine. 2017; 9(379):eaah4586. [PubMed: 28251904]

(37)Hussain S, Hess K, Gearhart J, Geiss K, Schlager J. In vitro toxicity of nanoparticles in BRL 3A rat liver cells Toxicology in vitro. 2005; 19(7):975–983. [PubMed: 16125895]

(38)Naqvi S, Samim M, Abdin M, Ahmed FJ, Maitra A, Prashant C, Dinda AK. Concentration-dependent toxicity of iron oxide nanoparticles mediated byincreased oxidative stress Int JNanomed. 2010; 5:983–989.

(39)Albanese A, Chan WC. Effect of gold nanoparticle aggregation on cell uptake and toxicity Acs Nano. 2011; 5(7):5478–5489. [PubMed: 21692495]

(40)Wu X, Tan Y, Mao H, Zhang M. Toxic effects of iron oxide nanoparticles on human umbilical vein endothelial cells Int J Nanomedicine. 2010; 5:385–399. [PubMed: 20957160]

(41)Guo X, Mao F, Wang W, Yang Y, Bai Z. Sulfhydryl-modified Fe3O4@ SiO2 core/shell nanocomposite: synthesis and toxicity assessment in vitro ACS applied materials & interfaces. 2015; 7(27):14983–14991. [PubMed: 26083720]

(42)Zou J, Peng Y-G, Tang Y-Y. A facile bi-phase synthesis of Fe 3 O 4@ SiO 2 core-shell nanoparticles with tunable film thicknesses RSCAdvances. 2014; 4(19):9693–9700.

(43)Zhang Y, Wei C, Zhang P, Li X, Liu T, Pu Y, Li Y, Cao Z, Cao H, Liu Y. Efficient reprogramming of naive-like induced pluripotent stem cells from porcine adipose-derived stem cells with a feeder-independent and serum-free system Plos One. 2014; 9(1):e85089. [PubMed: 24465482]

(44)Jay JM, Modern food microbiology Bioassay and Related MethodsSpringer; 1992 166184

(45)Karlsson HL, Gustafsson J, Cronholm P, Moller L. Size-dependent toxicity of metal oxide particles--a comparison between nano- and micrometer size Toxicology Letters. 2009; 188(2): 112–118. [PubMed: 19446243]

(46)Orynbayeva Z, Sensenig R, Polyak B. Metabolic and structural integrity of magnetic nanoparticle-loaded primary endothelial cells for targeted cell therapy Nanomedicine. 2015; 10(10):1555–1568. [PubMed: 26008193]

(47)Gozuacik D, Kimchi A. Autophagy as a cell death and tumor suppressor mechanism Oncogene. 2004; 23(16):2891–2906. [PubMed: 15077152]

(48)Wu X, Tan Y, Mao H, Zhang M. Toxic effects of iron oxide nanoparticles on human umbilical vein endothelial cells Int JNanomed. 2010; 5(1):385–396.

(49)Finken R, Seifert U. Wrinkling of microcapsules in shear flow Journal of Physics: Condensed Matter. 2006; 18(15):L185–L191.

(50)Ma M, Chiu A, Sahay G, Doloff JC, Dholakia N, Thakrar R, Cohen J, Vegas A, Chen D, Bratlie KM. Core-shell hydrogel microcapsules for improved islets encapsulation Adv Healthc Mater. 2013; 2(5):667–672. [PubMed: 23208618]

(51)Nguyen DK, Son YM, Lee NE. Hydrogel Encapsulation of Cells in Core-Shell Microcapsules for Cell Delivery Adv Healthc Mater. 2015; 4(10):1537–1544. [PubMed: 25963828]

(52)Huang H, Choi JK, Rao W, Zhao S, Agarwal P, Zhao G, He X. Alginate hydrogel microencapsulation inhibits devitrification and enables large - volume low - CPA cell vitrification Adv FunctMater. 2015; 25(44):6839–6850.

(53)Etheridge ML, Xu Y, Rott L, Choi J, Glasmacher B, Bischof JC. RF heating of magnetic nanoparticles improves the thawing of cryopreserved biomaterials Technology. 2014; 2(03):229–242.

(54)Sakai A, Kobayashi S, Oiyama I. Cryopreservation of nucellar cells of navel orange (Citrus sinensis Osb. var. brasiliensis Tanaka) by vitrification Plant Cell Reports. 1990; 9(1):30–33. [PubMed: 24226373]

(55)Yavin S, Aroyo A, Roth Z, Arav A. Embryo cryopreservation in the presence of low concentration of vitrification solution with sealed pulled straws in liquid nitrogen slush Human Reproduction. 2009; 24(4):797–804. [PubMed: 19141483]

(56)Food, U.; Administration, D. Guidance for FDA reviewers and sponsors: Content and review of chemistry, manufacturing, and control (CMC) information for human somatic cell therapy investigational new drug applications (INDs). Washington, DC: US Food and Drug Administration 2008.

(57)Zvibel I, Smets F, Soriano H. Anoikis: roadblock to cell transplantation? Cell transplantation. 2002; 11(7):621–630. [PubMed: 12518889]

(58)Terry C, Hughes RD, Mitry RR, Lehec SC, Dhawan A. Cryopreservation-induced nonattachment of human hepatocytes: role of adhesion molecules Cell transplantation. 2007; 16(6):639–647. [PubMed: 17912955]

(59)Vieira NM, Brandalise V, Zucconi E, Secco M, Strauss BE, Zatz M. Isolation, characterization, and differentiation potential of canine adipose-derived stem cells Cell Transplantation. 2010; 19(3):279–289. [PubMed: 19995482]

(60)Huang SJ, Fu RH, Shyu WC, Liu SP, Jong GP, Chiu YW, Wu HS, Tsou YA, Cheng CW, Lin SZ. Adipose-derived stem cells: isolation, characterization, and differentiation potential Cell Transplantation. 2013; 22(4):701–709. [PubMed: 23068312]

(61)Morris GJ, Acton E, Avery S. A novel approach to sperm cryopreservation Human Reproduction. 1999; 14(4):1013–1021. [PubMed: 10221235]

(62)Zhang Y, Zhao G, Hossain SC, He X. Modeling and experimental studies of enhanced cooling by medical gauze for cell cryopreservation by vitrification International Journal of Heat and Mass Transfer. 2017; 114:1–7. [PubMed: 29398719]

(63Huang H, Zhao G, Zhang Y, Xu J, Toth TL, He X. Predehydration and Ice Seeding in the Presence of Trehalose Enable Cell Cryopreservation ACS Biomaterials Science & Engineering. 2017; 3(8):1758–1768. [PubMed: 28824959]

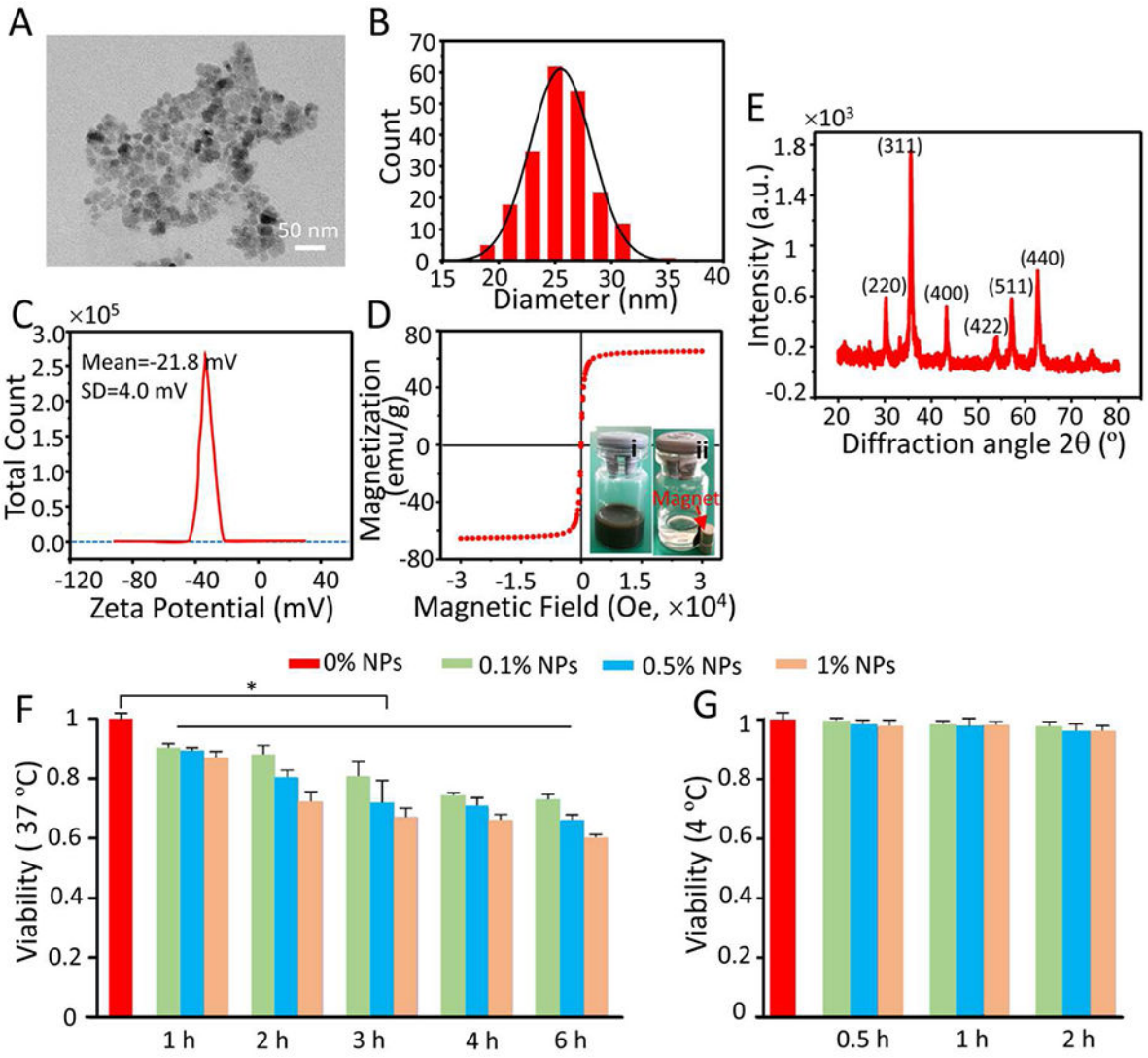

Figure 1.

Characterization and cytotoxicity of Fe_3O_4 NPs. A) Representative TEM images of Fe_3O_4 NPs. B) Size distribution of Fe_3O_4 NPs quantified by dynamic light scattering (DLS) at room temperature. C) Zeta potential of Fe_3O_4 NPs measured at room temperature. D) Magnetization curve of Fe_3O_4 NPs quantified by superconducting quantum interference device (SQUID) at room temperature. The insets (i) and (ii) show typical images of the Fe3O4 NPs dispersed in deionized water before and after applying magnetic field using a magnet, respectively. E) X-ray diffraction (XRD) pattern of Fe_3O_4 NPs. F-G) Cytotoxicity of the Fe_3O_4 NPs detected by the CCK-8 assay at 37 °C (F) and 4 °C (G) after different incubation times. Time- (1, 2, 3, 4, and 6 h) and concentration-dependent (0.1, 0.5, and 1% (w/v)) cytotoxicity was observed at 37 °C, but no cytotoxicity was observed after the cells were treated with different concentrations (0.1, 0.5, and 1% (w/v)) of NPs for 0.5, 1, and 2 h at 4 °C.

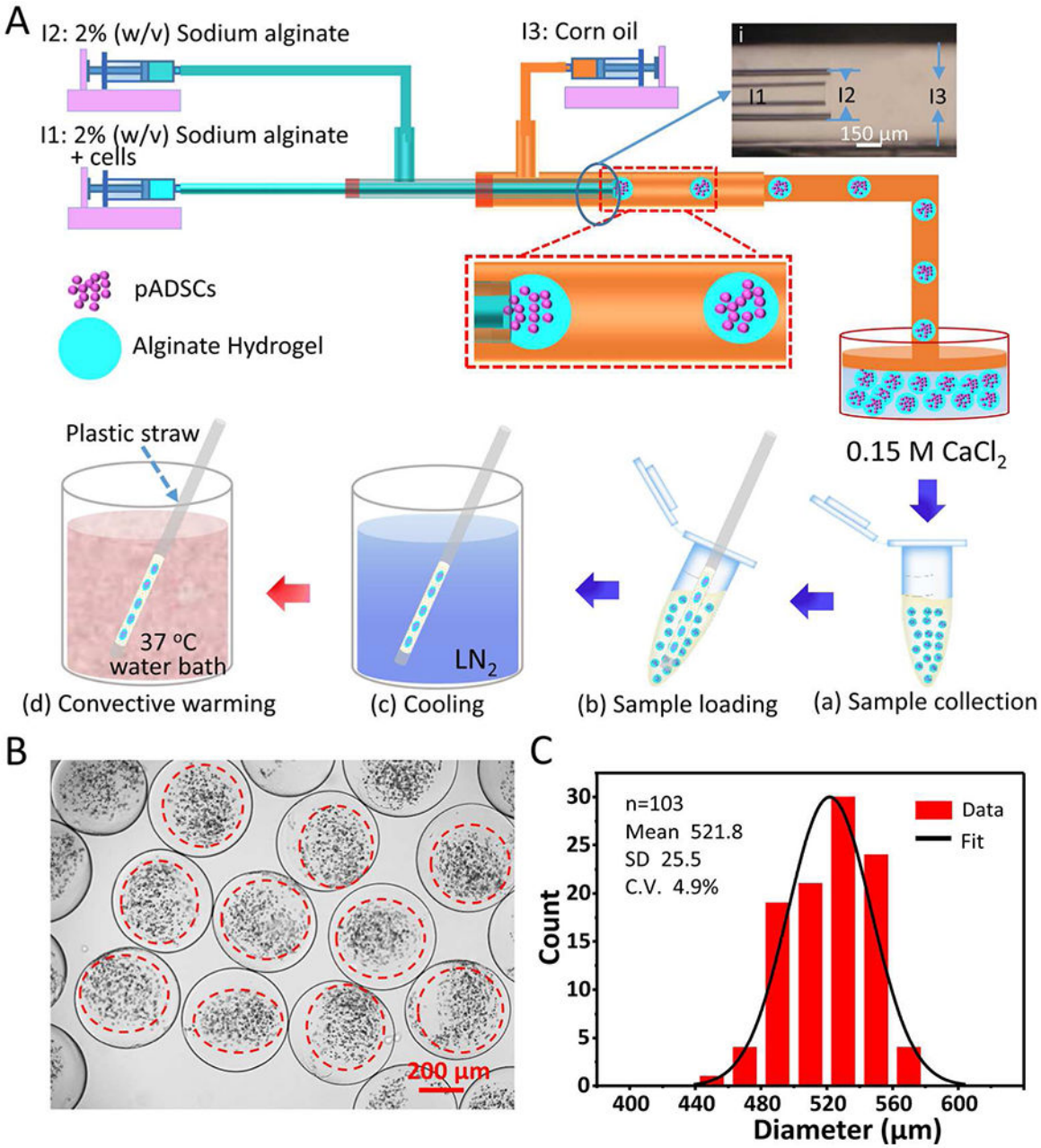

Figure 2.

A schematic illustration of generating cell-alginate hydrogel biocomposites by using a tube-in-tube capillary microfluidic device and the procedure of vitrificaiton with warming at 37 °C in water bath. A) An overview of the device and procedure for generating microcapsules and the procedure for vitrification with warming at 37 °C in water bath. (i) A micrograph showing the configuration of the tube-in-tube capillary device, and the sketches in (a-d) illustrate the process of vitrification with warming at 37 °C in water bath. B-C) Typical differential interference contrast (DIC) images and diameter distribution of microcapsules generated using the tube-in-tube capillary microfluidic device in this study.

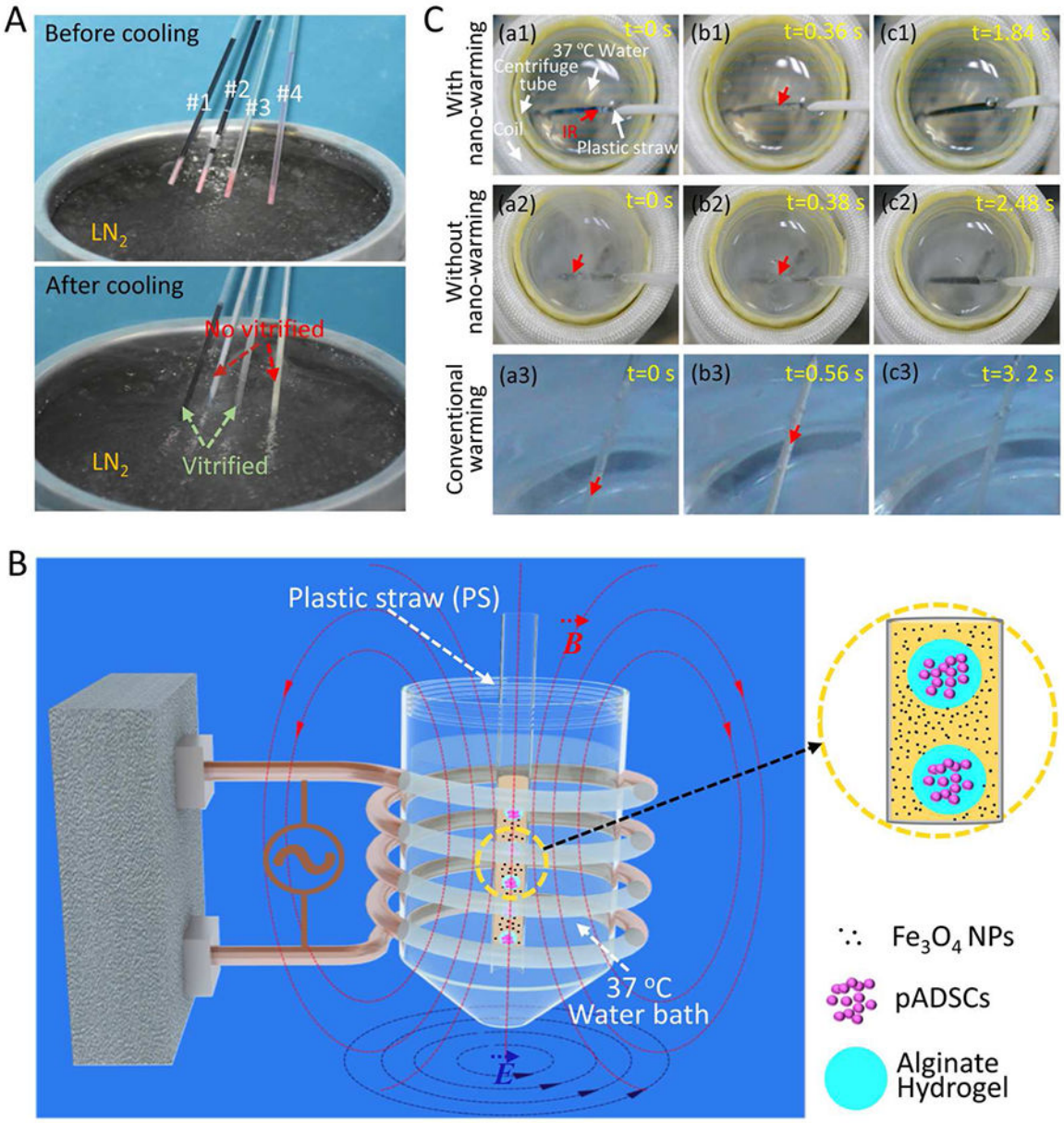

Figure 3.

The processes of cooling, nano-warming by magnetic induction heating (MIH) of Fe_3O_4 NPs, and conventional warming. A) Typical pictures showing the appearance of CPA solution (1 M DMSO, 1 M EG, and 1.3 M trehalose) or culture medium either with (PS #1 and PS #2) or without (PS #3 and PS #4) 0.5% Fe_3O_4 NPs in plastic straws (PS) before and after cooling by plunging into liquid nitrogen (LN2) without warming. B) A PS loaded with cell-alginate hydrogel constructs and NPs in CPA solution is taken out of liquid nitrogen and immediately plunged into a centrifuge tube with 37 °C water in the coil. The magnitude of the magnetic field can be adjusted by changing the current intensity of the AC field to control the warming process. C) Devitrification/recrystallization occurred during nano-warming (a1-c1) and conventional warming (with and without NPs, a2-c2 and a2-c3). If the

beginning time of devitrification/recrystallization was set as 0 s in a1, a2 and a3, the corresponding devitrification/recrystallization was completed at 0.36, 0.38, and 0.56 s as shown in b1, b2, and b3, respectively. The ice melted completely at 1.84, 2.48 and 3. 2 s as shown in c1, c2, and c3, respectively. IR: Ice recrystallization.

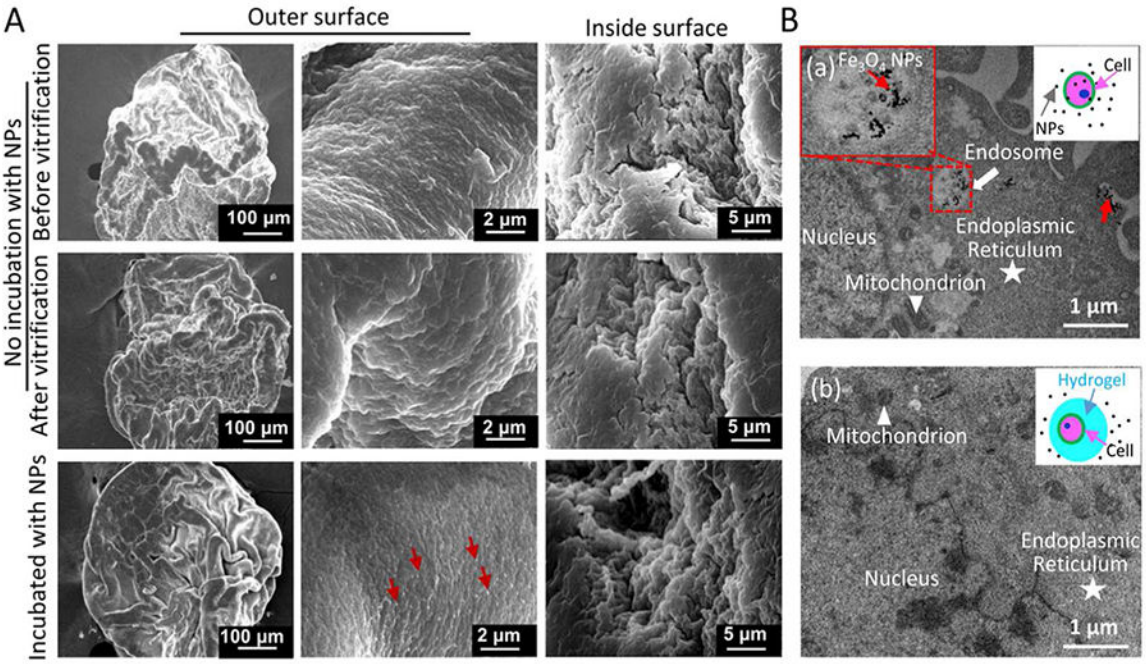

Figure 4.

SEM images of cell-alginate hydrogel constructs under different conditions and cell uptake of Fe3O4 NPs. A) No evident difference in the morphology of hydrogel microcapsules before and after vitrification with nano-warming. When the constructs (microcapsules) were incubated with Fe3O4 NPs overnight at 4 °C, the NPs appeared only on the surface of the microcapsules. The red arrow indicates Fe_3O_4 NPs. B) Non-encapsulated pADSCs (a) and pADSCs-hydrogel constructs (b) were incubated with Fe_3O_4 NPs for 10 h at 37 °C. The NPs were only found in non-encapsulated cells (a), the red arrow indicates NPs in endosomes.

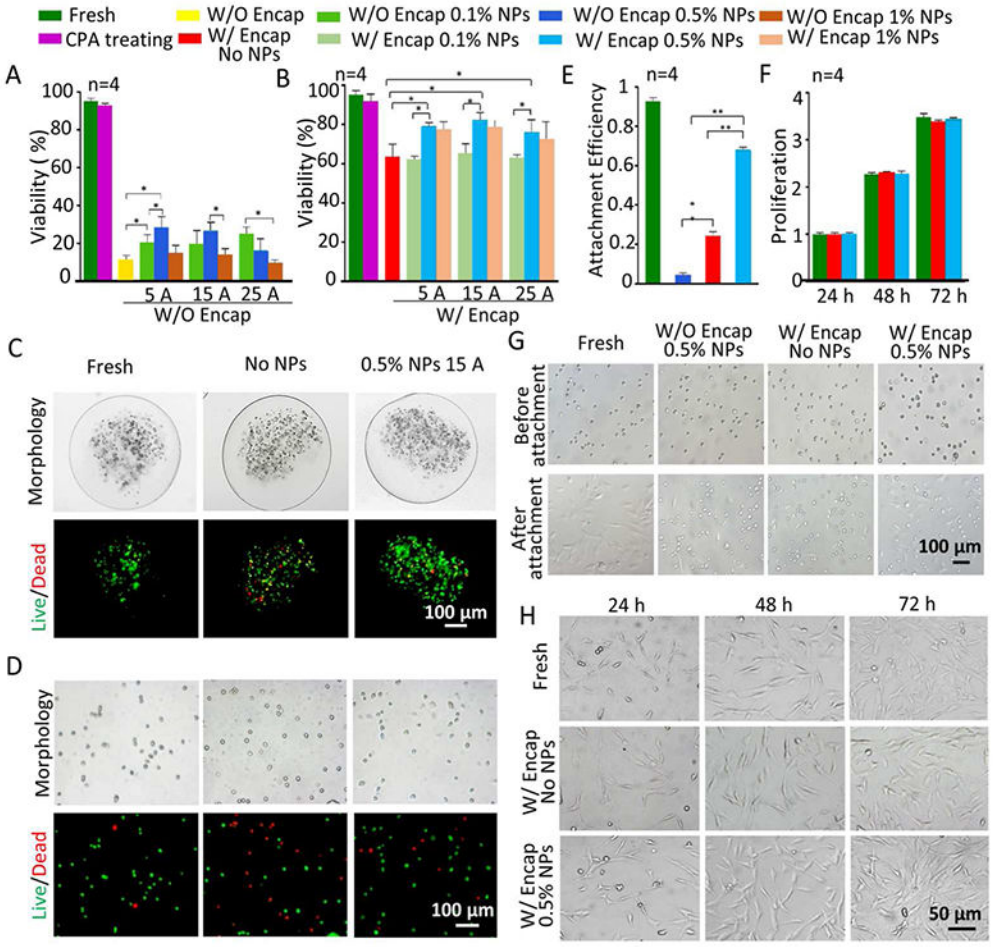

Figure 5.

Cell viability, attachment efficiency, and proliferation of pADSCs post-vitrification under different conditions. Viability of non-encapsulated pADSCs (A) and encapsulated pADSCs (B) under different conditions, *i.e.*, fresh, CPA treated, and post-vitrification without or with three different concentrations of NPs with nano-warming by MIH under an AC magnetic field (5 A, 15 A and 25 A). C) Typical DIC and fluorescence images show the morphology and viability of pADSCs in microcapsules under three different conditions, *i.e.*, fresh and post-cryopreservation without NPs and with 0.5% NPs with nano-warming by MIH under an AC magnetic field (15A). D) Typical DIC and fluorescence images showing the morphology and viability of pADSCs released from microcapsules post-vitrification under the same three conditions in (C). E) The attachment efficiency of non-encapsulated and microencapsulated pADSCs post-vitrification with or without nano-warming by MIH of 0.5% Fe_3O_4 NPs (15 A). F) The proliferation of microencapsulated pADSCs post-vitrification without or with nano-warming by MIH of 0.5% Fe_3O_4 NPs (15 A). G) Representative images of pADSC attachment under the aforementioned conditions. H) Representative images of pADSC proliferation under different conditions. Red: dead and green: live. *: $p < 0.05$. **: $p < 0.01$. W/O Encap: without encapsulation and W/ Encap: with encapsulation.

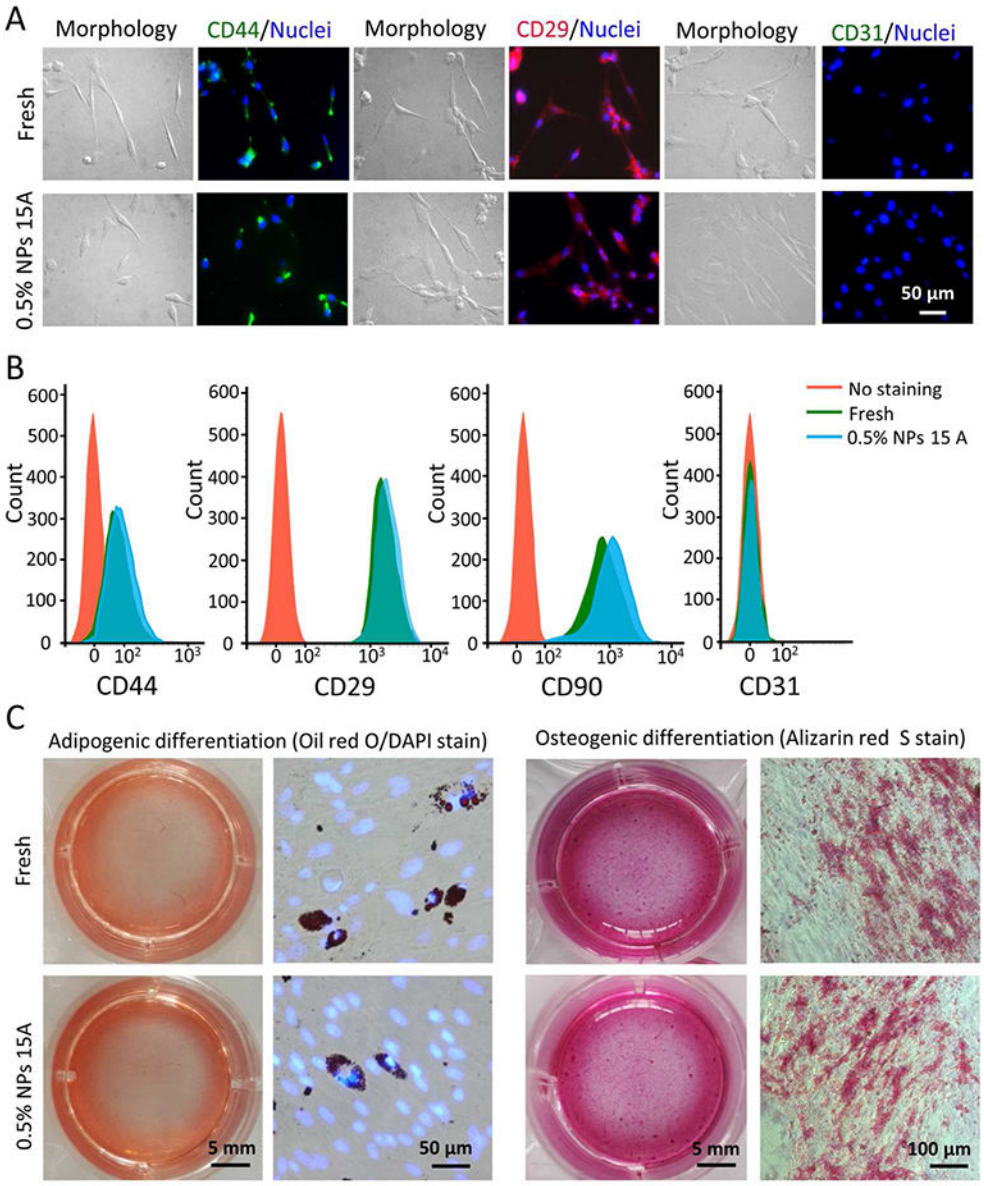

Figure 6.

Function of pADSCs post-vitrification with nano-warming (15 A and 0.5% Fe_3O_4 NPs). A) Fluorescence immunostaining images of CD44 (+), CD29 (+), and CD31 (−) showing the expression of the three markers on the pADSCs. B) Quantification of CD44 (+), CD29 (+), CD90 (+), and CD31 (−) expression on the pADSCs by flow cytometry. C) Qualitative assessment of adipogenic and osteogenic differentiation of fresh and cryopreserved pADSCs.

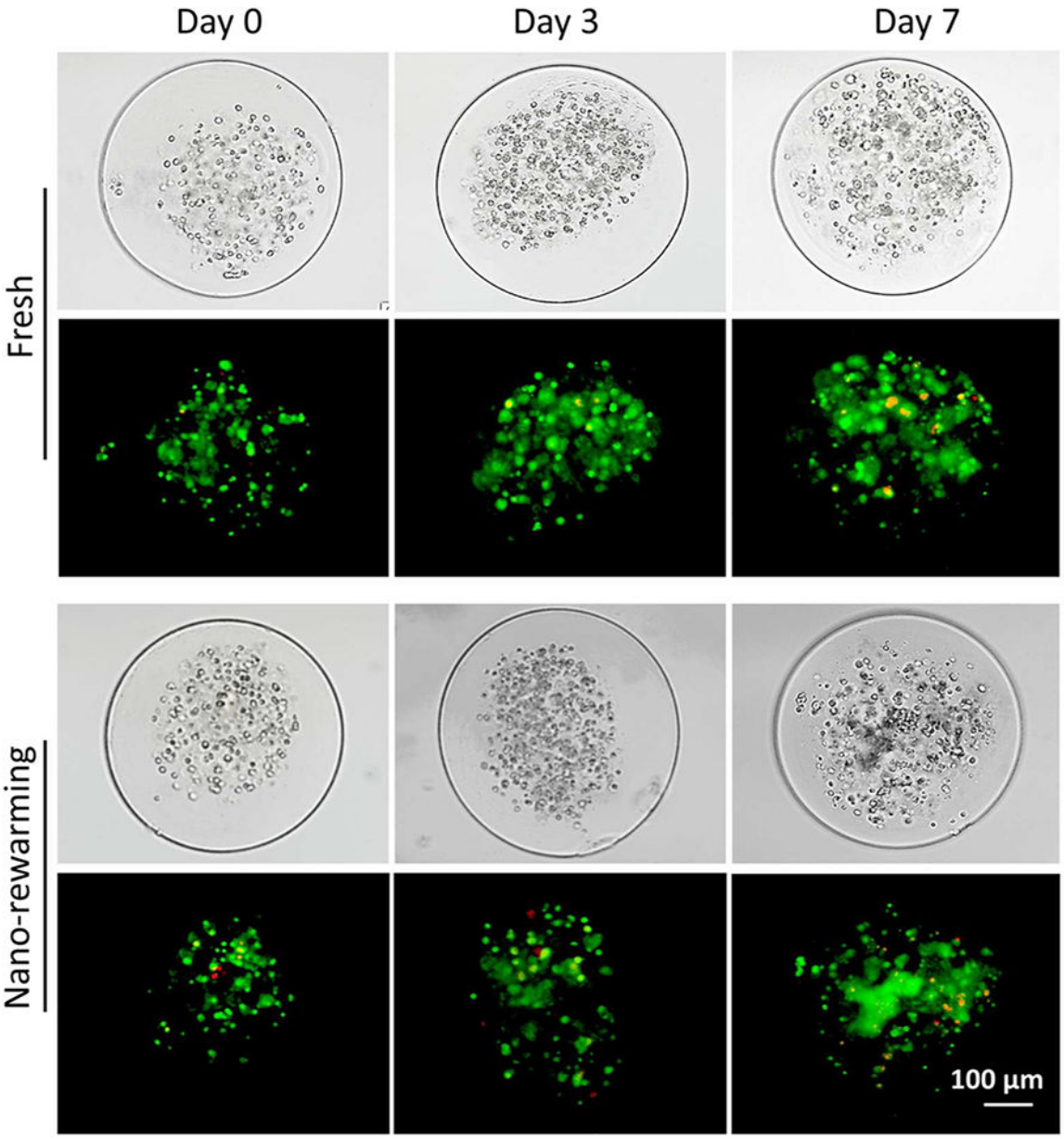

Figure 7.

Viability and proliferation of pADSCs in cell-alginate hydrogel constructs post-vitrification under 3D culture. Both typical DIC images of pADSCs in fresh and post-vitrification constructs on days 0, 3 and 7 under 3D culture, and the corresponding fluorescence images show high viability of pADSCs in the constructs are shown. Red: dead and green: live.

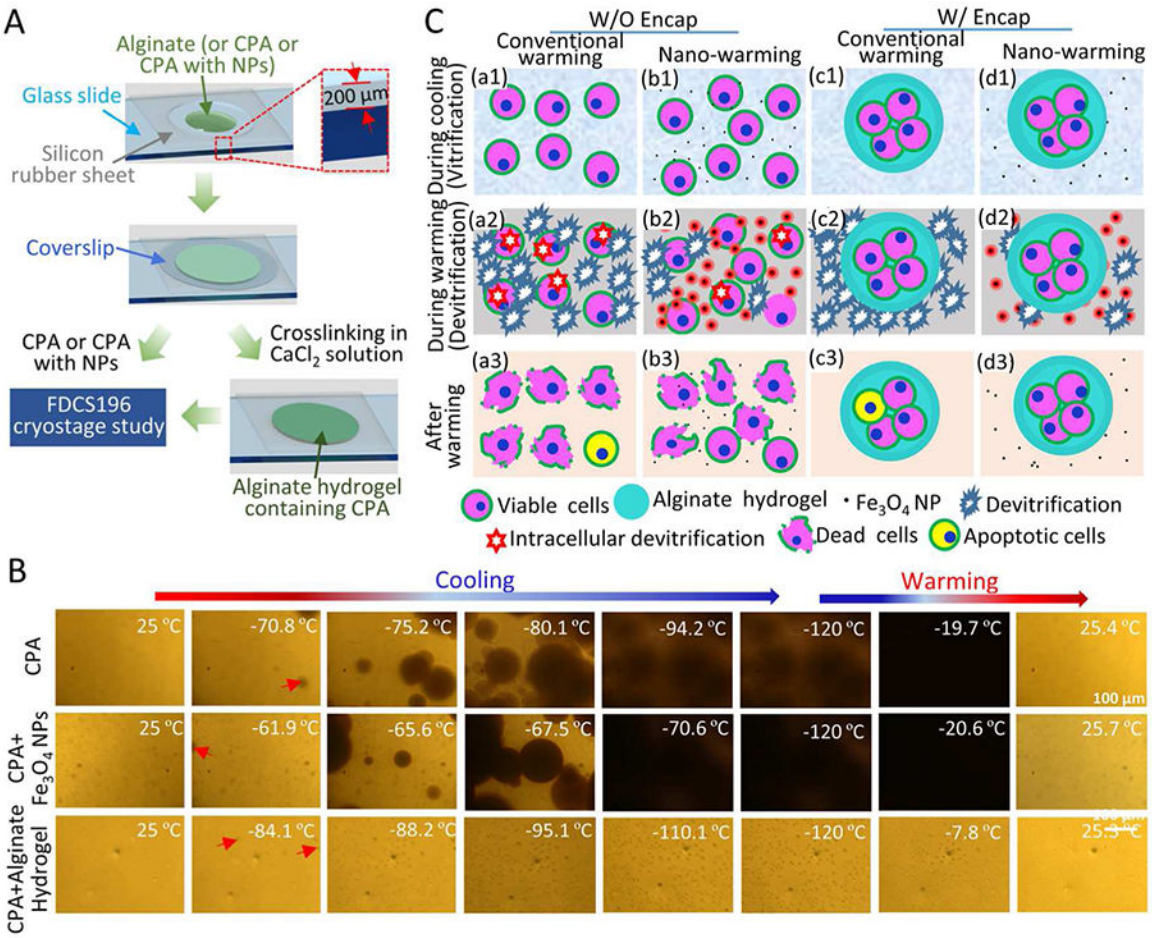

Figure 8.

Cryomicroscopic analysis and a schematic illustration of the possible mechanisms of enhancing cell vitrification by alginate hydrogel microencapsulation and nano-warming. A) Sample preparation for cryomicroscopic studies. A silicone film and coverslip are used to keep the thickness of experimental sample, including CPA, Fe_3O_4 NPs with CPA, and alginate hydrogel containing CPA. B) Typical images showing the freezing and warming processes of CPA solution, CPA solution with Fe_3O_4 NPs, and alginate hydrogel containing CPA. The red arrows indicate initial ice crystals. For the aforementioned three samples, the ice crystals appear at −70.8 °C, −61.9 °C and −84.1 °C, and continue to grow till −94.2 °C, −70.6 °C and −95.1 °C, respectively. Recrystallization occurs at −19.7 °C and −20.6 °C during warming CPA solution and CPA solution with NPs, respectively. Recrystallization does not occur during warming of alginate hydrogel containing CPA solution. C) Cells and cell-alginate hydrogel constructs at three different stages of the vitrification cryopreservation procedure: during cooling (a1-d1), during warming (a2-d2), and after warming (a3-d3). The alginate hydrogel microencapsulation may enhance vitrification during cooling and reduce devitrification/recrystallization during warming. The latter is further minimized by nano-warming *via* both the selective local and global heating effect of the Fe3O4 NPs under

magnetic field. The nano-warming is crucial for cryopreservation of large cell-alginate hydrogel constructs by low-CPA vitrification.